# Nicotianamine synthase activity affects nucleolar iron accumulation and impacts rDNA silencing and RNA methylation in Arabidopsis

Charlotte Montacié, Christophe Riondet, Lili Wei, Tommy Darrière, Alizée Weiss, Frédéric Pontvianne, Marie-Line Escande, Anne de Bures, Edouard Jobet, A. Barbarossa, et al.

# *NICOTIANAMINE SYNTHASE* activity affects nucleolar iron accumulation and impacts rDNA silencing and RNA methylation in Arabidopsis

Montacié C.[1,2], Riondet C.[1,2], Wei L.[3], Darriere T.[1,2], Weiss A[1,2], Pontvianne F.[1,2], Escande M.L.[4,5], de Bures A.[1,2], Jobet E.[1,2], Barbarossa A.[1,2], Carpentier M.C.[1,2], Aarts M.G.M.[6], Attina A[7]., Hirtz C.[7], David A.[8], Marchand V.[9], Motorin Y.[9,10], Curie C. [3], Mari S.[3], Reichheld J-P.[1,2], and Sáez-Vásquez J.[1,2]

[1]CNRS, Laboratoire Génome et Développement des Plantes (LGDP), UMR 5096, 66860 Perpignan, France.

[2]Univ. Perpignan Via Domitia, LGDP, UMR 5096, 66860 Perpignan, France.

[3]BPMP, Université Montpellier, CNRS, INRAE, Institut Agro, Montpellier F-34060, France

[4]CNRS, Observatoire Océanologique de Banyuls s/ mer, 66650 Banyuls-sur-mer, France

[5]BioPIC Platform of the OOB, 66650 Banyuls-sur-mer, France

[6]Laboratory of Genetics, Wageningen University & Research, 6700AA Wageningen, Netherlands

[7]IRMB, Univ. Montpellier, INSERM, CHU Montpellier, CNRS, Montpellier, France

[8]IGF, Univ. Montpellier, CNRS, INSERM, Montpellier, France

[9]Université de Lorraine, CNRS, INSERM, IBSLor, (UMS2008/US40), Epitranscriptomics and RNA Sequencing (EpiRNA-Seq) Core Facility, F-54000 Nancy, France

[10]Université de Lorraine, CNRS, IMoPA (UMR 7365), F-54000 Nancy, France

**Highlight:** Low iron in the nucleolus and RNA modification changes suggest a central role of nicotianamine synthesis in rRNA gene expression.

**Abstract**

In plant cells, a large pool of iron (Fe) is contained in the nucleolus, together with that in chloroplasts and mitochondria. A central determinant for intracellular distribution of Fe is nicotianamine (NA) generated by NICOTIANAMINE SYNTHASE (NAS). Here, we characterized *Arabidopsis thaliana* plants with disrupted *NAS* genes to modify accumulation of nucleolar iron and understand its role in nucleolar functions and more specifically in rRNA gene expression. We found that *nas124* triple mutant plants, which contain lower quantities of the iron ligand NA, also contain less iron in the nucleolus. This is concurrent with the expression of normally silenced rRNA genes from Nucleolar Organizer Regions 2 (NOR2). Notably, in *nas234* triple mutant plants, which also contain lower quantities of NA, nucleolar iron and rDNA expression are not affected. In contrast, in both *nas124* and *nas234*, specific RNA modifications are differentially regulated in a genotype dependent manner. Taken together the data point out the impact of specific NAS activities in RNA gene expression. We discuss the interplay between NA and nucleolar iron with rDNA functional organization and RNA methylation.

**Keywords:** nicotianamine, iron, nucleolus, rDNA, methylation, redox

**Abbreviations:** Nicotianamine (NA), NICOTIANAMINE SYNTHASE (NAS), Nucleolar Organizer Regions (NORs), S-adenosyl-methionine (SAM), 3,3'-diaminobenzidine (DAB), Reactive oxygen species (ROS), Glutaredoxin 1 (GRX1), Fibrillarin 2 (Fib2), Nitro blue tetrazolium chloride (NBT), OLIGOPEPTIDE TRANSPORTER, (OPT3), IRON REGULATED TRANSPORTER 3 (IRT3), Transmission Electron Microscopy (TEM), Fibrillar centers (FC), Dense Fibrillar Components (DFC), Granular Component (GC), rRNA and rDNA (ribosomal RNA and RNA), Fluorescence *In Situ* Hybridization (FISH), Chromatin Immuno-Precipitation (ChIP), LC-MRM (liquid chromatography-multiple reaction monitoring), RiboMethSeq (RNA 2'-O-methylation sequencing).

## Introduction

The nucleolus is a multifunctional structure linked to ribosome biogenesis, assembly of ribonucleoprotein complexes, nuclear chromatin organization, sequestering of proteins and stress response (Boulon *et al.*, 2010; Hernandez-Verdun *et al.*, 2010; Pederson and Powell, 2015; Stepinski, 2014; Tsai and Pederson, 2014; Tsekrekou *et al.*, 2017).

The plant nucleolus has an additional, and less investigated role as a pool of iron and for its intracellular distribution (Roschzttardtz *et al.*, 2011). Iron is one of the most important micronutrients in plants, implicated in almost every cellular process. Iron excess or deprivation lead to severe growth phenotypes in plants, decrease in biomass production and chlorosis of leaves (Briat *et al.*, 2015). Accumulation of iron in the nucleolus is intriguing also from the perspective that several neurodegenerative diseases are related to nucleolar iron in human cells (Heeney and Finberg, 2014; Kumar *et al.*, 2016) (Quintana *et al.*, 2006). In Alzheimer's disease, iron damages DNA (Henle *et al.*, 1999; Henle *et al.*, 1996) and binds directly to ribosomal RNA (rRNA), as well as ribosomes, leading to their oxidation and impacting translation efficiency (Honda *et al.*, 2005). Despite these deleterious effects of nucleolar iron, recent studies point out a regulatory role of iron on ribosome assembly and function under specific cellular conditions. The ribosome is particularly dependent on $Mg^{2+}$ to fold and maintain stability due to the negative charge of the rRNA backbone. However, ribosomal $Mg^{2+}$ can be substituted with other divalent cations, including $Fe^{2+}$ and the ribosome can competently mediate translation in this state (Bray *et al.*, 2018; Smethurst *et al.*, 2020; Smethurst and Shcherbik, 2021). Notably, while $Fe^{2+}$ interactions with the ribosome were relevant in ancient ribosomes (containing $Mg^{+2}$ before the evolution of photosynthesis and the increase in molecular oxygen), little is known how iron impact nucleolus organization and ribosome synthesis in the present-day oxidative environmental conditions.

Nicotianamine (NA) is a key ligand for essential metals, including iron (Curie and Briat, 2003). NA is an amino acid derivative, synthesized from three S-adenosyl-methionine (SAM) moieties by NICOTIANAMINE SYNTHASE (NAS) (Figure 1A and references in (Klatte *et al.*, 2009)). The genome of *A. thaliana* contains four NAS genes (Bauer *et al.*, 2004). In the quadruple *nas* mutant (*nas4x-2*) NA is not detectable in rosette leaves; also the *nas4x-2* shows a chloronerva-like phenotype and is sterile (Klatte *et al.*, 2009).

Here, we demonstrate that in specific Arabidopsis *nas* mutant plants the nucleolar localization of iron is inhibited. Concomitant, in these *nas* mutants, rDNA genes from normally silenced NOR2 are expressed and RNA and methylation profiles changed. We discuss how inhibition of NAS activity might affect rDNA gene expression and/or methylation of RNAs.

## Materials and methods

### *Plant material and growth conditions*

All lines were derived from *Arabidopsis thaliana* Columbia-0 ecotype. Seeds corresponding to *nas1-2* (SALK_082174), *nas1-1* (GK223A09), *nas2-2* (SALK_066962), *nas3-2* (SALK_106467) and *nas4-1* (SALK_135507) mutant plants were obtained from the Nottingham Arabidopsis Stock Centre (http://nasc.life.nott.ac.uk). Crosses between single homozygous T-DNA (SALK) insertion lines were performed to generate triple homozygous mutants, and were identified by PCR and RT-PCR

(Supplementary Fig. S1). The *nuc1-2* was previously described (Durut *et al.*, 2014; Pontvianne *et al.*, 2010).

Plants were grown either on soil for 21 days, or *in vitro* on 1X Murashige and Skoog medium (Duchefa Biochemie M0231, including Gamborg B5 vitamins, supplemented with 0,05% (w/v) MES and 1% (w/v) plant agar (pH was adjusted at 5,7 with KOH) for 15 days. For the soil grown plants, only the aerial parts were collected for analysis, whereas for the *in vitro* conditions the whole seedlings were analyzed. Plants were grown under an 8h/16h photoperiod (dark/light) at 21°C.

### *Nicotianamine (NA) analysis*

Approximately 0.1g of fresh 15 days-old *in vitro* plants were ground to a fine powder in liquid nitrogen and analyzed for NA amount by RP-HPLC with pre-column derivatization with *o*-phtalaldialdehyde, as previously described (Klatte *et al.*, 2009).

### *Molecular Cloning and Plasmid Constructs.*

For construction of the Fib2-roGFP plasmid, the GAR domain (amino acids 1-73) of the Arabidopsis Fibrillarin 2 (Fib2) gene was PCR amplified with Phusion polymerase (Finnzymes) using the primers *Fib2_KpnI* and *Fib2_BamH1* to add KpnI and BamHI restriction sites (Supplementary Table S5). The PCR product was cloned blunt-end into the vector pGEM-T (Promega). The GAR domain was then subcloned into the expression vector pBinAR-GRX1-roGFP2 (Marty *et al.*, 2009) with KpnI and BamHI. The construct was transformed into the Agrobacterium strain C58C1 and used for Arabidopsis transformation.

### *Confocal Laser-Scanning Microscopy and redox ratio analysis*

Confocal microscopic observations were carried out using the Axio observer Z1 microscope with the LSM 700 scanning module and the ZEN 2010 software (Zeiss). Excitation of roGFP2 was performed at 488 and 405 nm and a bandpass (BP 490-555 nm) emission filter was used to collect roGFP2 signal. For background subtraction, signal was recovered using a BP 420-480 nm emission filter during excitation at 405 nm. Image analyses and quantifications were performed as previously described (Gutscher et al., 2008), using the public domain image analysis program ImageJ 1.52i (https://imagej.nih.gov/ij/).

### *Cleared cotyledons and Perls/DAB staining*

For vein pattern, cotyledons from 10 days-old WT, *nas124* and *nas234 in vitro* seedlings were cleared in a 3:1 ethanol:acetic acid (v/v) solution, rinsed and conserved in 70% ethanol and observed under dark-field illumination. For Perls/DAB staining, leaf fragments from 15 days-old *in vitro* seedlings were vacuum-infiltrated with the fixation solution containing 2% (w/v) paraformaldehyde, 1% (v/v) glutaraldehyde, 1% (w/v) caffeine in 100 mM phosphate buffer (pH 7). The fixed samples were treated and analyzed for Fe histochemical staining according to (Roschzttardtz *et al.*, 2009). Vein pattern and Pearls/DAB observations were performed using LEICA MZ12 and DFC425 Digital Microscope camera systems.

## *Transmission Electron Microscopy (TEM)*

Roots from 5, 10 and 15 day old plants, *in vitro* grown, were first fixed with 3% (v/v) glutaraldehyde in 0.025M cacodylate buffer (pH7.3) at room temperature. After washing, the samples were post-fixed with 1% OsO4 in the same buffer. The samples were then dehydrated in a methanol series (30, 50, 70 and 100%) at room temperature. The samples were acetylated and methylated with a freshly prepared 5:1 (v/v) methanol/acetic anhydride mixture at 25°C. Samples were then washed in pure methanol and embedded in Epon 812 resin (Sigma). Ultrathin sections were performed on an ultra-microtome (Leica Ultracut), and counterstained with uranyl acetate and lead citrate before being observed using a 7500 Hitachi TEM.

## *Fluorescence In Situ Hybridization (FISH)*

The FISH probe containing intergenic spacer (IGS) and 5'external transcribed spacer (5'ETS) rDNA sequences (-220/+250) was amplified with primers *o112/o113* (Supplementary Table S5) and cloned in pGEM-T® vector (Promega) and amplified by PCR using universal primers T7/M13R and supplying biotin-16-dUTP (Roche, Meylan, France) to the reaction. The analysis was performed using nuclei from leaves of 21 day-old plants grown on soil. The biotin labeled probe was detected using digoxigenin (1:200; Roche) followed by sheep anti-digoxigenin antibody conjugated with the fluorochrome Alexa 480 (1:200; Invitrogen). Slides were prepared using Vectashield (Vector Laboratories) mounting medium supplemented with 1µg/mL DAPI (4',6-diaminido-2-phenylindole) and then observed by confocal microscopy (LSM700 scanning microscope, Zeiss).

## *DNA and RNA isolation*

DNA was extracted from liquid nitrogen ground powder by using the DNeasy® plant Mini Kit (Qiagen). The DNA extraction with illustra™ Nucleon™ PhytoPure™ (GE Healthcare) was specifically used to prepare DNA for bisulfite analysis. For RNA, around 800 µL of frozen powder were supplemented with 5 mL of Tri Reagent® (Molecular Research Center, Inc), then 1 mL of cold chloroform was added. After a 3 minutes incubation, the mix was centrifuge at 8,000 *g* for 15 min at 4°C. Then 3 mL of cold isopropanol was added to the conserved aqueous phase and the resulting product was then centrifuged at 8,000 *g* for 30min at 4°C. Isopropanol was replaced by 75% ethanol and the mix was incubated overnight at -20°C. The pellet was dried and resuspended in 65°C DEPC-treated water. DNA was removed from samples by using the TURBO DNA-free™ kit (Invitrogen), according to the manufacturer's instructions.

## *PCR, RT-PCR and qPCR*

RT-PCR reactions were performed using SuperSript IV Reverse Transcriptase (ThermoFisher Scientific). For cDNA production we used simultaneously random and oligo dT primers. The protocol was performed following the manufacturer's instructions. The cDNA obtained were used for PCR experiments afterwards. PCR amplifications were made using the GoTaq® DNA Polymerase and 5X GoTaq® Green buffer (Promega). 3'ETS products from RT-PCR and PCR reactions were loaded on an agarose gel (2% agarose) in TAE 0,5X supplemented with Gel Red. Quantitative PCR (qPCR) was performed using a LightCycler 480 and MESA Blue qPCR Master Mix Plus for SYBR assay (Eurogentec)

in compliance with manufacturer procedures. All primer pairs used in RT-PCR, PCR and qPCR are provided in Supplementary Table S5.

### *Bisulfite DNA treatment and analysis*

DNA was converted (me5C to T) using the EpiTect Plus Bisulfite Conversion kit (Qiagen). The target region was then amplified by PCR using the kit Ex Taq DNA polymerase, hot start version (TaKaRa Bio Inc.) and oligo primers *o112/o113* and *o124/o125* (Supplementary Table S5) to amplify respectively promoter/5'ETS and 3'ETS. 3'ETS PCR products were run on an agarose gel, sliced from the gel and purified using GeneClean® Turbo kit (MP Biomedicals). PCR products were cloned in pGEM®-T easy vector (Promega), transformed into *E. coli* DH5α, and sequenced using T7 and SP6 primers. The sequences obtained were mapped to a reference sequence and the alignment was sent to CyMATE to analyze methylation sites in the sequence. The results were analyzed using prop.test function to verify significant differences with R software (Pontvianne *et al.*, 2012).

### *RiboMethSeq and detection of nucleosides using MRM method in mass spectrometry.*

RiboMethSeq analysis was performed using the method described in (Marchand et al. 2016) and recently used in Arabidopsis plants (Azevedo-Favory *et al.*, 2021).

Enzymatic processing of RNA: 400ng of total RNA from 15 day old *in vitro* grown WT, *nas124* and *nas234* plants were digested with 0.001U of Nuclease P1 (Sigma, N8630) and 3µL of 0.1M ammonium acetate pH5.3 during 2 hours at 42°C. Then a dephosphorylation of nucleosides was performed with 0.001U of alkaline phosphatase (Sigma, P4252) and 3µL of 1M ammonium acetate during 2 hours at 37°C. Next, the mixture was diluted twice and was filtered with 0.22µm filters (Millex®-GV, Millipore, SLGVR04NL). 5µL of each sample was injected in triplicate in a LC-MSMS and then estimated methylated/unmethylated ratios were stimated. Since the adenosine signal is saturated in the samples, we have used uridine (U) to estimate ratios (Supplementary Information S1).

### *RNA-seq and bioinformatics analyses*

Total RNA from 15 days-old *in vitro* grown WT or *nas124* mutant plants was prepared independently to generate three biological replicates per sample. Sequencing was performed by the POPS facility (Institut de Génomique-CNS, Evry, France) from stranded ribozero RNA-seq libraries and using NextSeq500 (Illumina) and Hiseq2000 to generate 2X 75bp long reads. Raw reads were trimmed using Trimmomatic v0.39 (Bolger et al., 2014). Trimmed reads were filtered out read corresponding to mitochondrial, chloroplastic and rRNA sequences using bowtie2 v2.3.5 (Langmead and Salzberg, 2012) in 'sensitive-local' mode. Reads mapping against TAIR10 genome with Araport11 gtf file was performed using Hisat2 v2.1.0 (Kim *et al.*, 2015). Read counting was performed using htseq-count v0.12.4 (Anders *et al.*, 2015) in 'union' mode and normalized by total of mapped reads (reads per millions, rpm). Differential analysis was performed using Bioconductor R v4.1.2 package DESeq2 (Love *et al.*, 2014) with a false discovery rate of 0.05. P values were corrected for multiple tests by the Benjamini-Hochberg rule (adjusted P value). The upregulated genes were defined with a fold change minimum to 2 and the downregulated genes with a fold change inferior to 1. The heat map was obtained using heatmap.2 function of gplots R package (https://CRAN.R-

project.org/package=gplots) using Pearson distance and an average method for the hierarchical clustering. To identify DE lncRNAs, Col-0 and *nas124* Illumina reads were aligned to the Arabidopsis Transcriptome ReconstructoR pipeline (https://doi.org/10.1101/2020.12.10.418897). All WT and *nas124* sequences were submitted to the Sequence Read Archive (SRA): PRJNA782822. https://dataview.ncbi.nlm.nih.gov/object/PRJNA782822?reviewer=ee044uijk32bst5p1v52bogou9. Gene Onthology (GO) analysis was performed using PANTHER (http://www.pantherdb.org/).

## Results

### *Plant phenotype and NA accumulation in nas124 and nas234 plants*

The genome of *A. thaliana* contains four *NAS* genes that are differentially expressed. *NAS1, NAS2* and *NAS4* are essentially expressed in roots, while *NAS3* is expressed at a low level in roots and leaves. Single T-DNA insertion lines do not show any visible phenotype (Bauer *et al.*, 2004) and have WT-nicotianamine levels (Klatte *et al.*, 2009). We characterized first the *nas124* and *nas234* triple mutant plants obtained from single *nas1-2* (SALK_082174), *nas2-2* (SALK_066962), *nas3-2* (SALK_106467) and *nas4-1* (SALK_135507) mutant plants (Supplementary Fig S1A and B).

The *nas124* and *nas234* triple mutants grown on soil do not show growth and/or plant developmental defects compared to the WT plants, though the first leaves from *nas124* grown *in vitro* display a chloronerva-like phenotype (Figure 1B). Cleared cotyledons from *nas124* and *nas234* show disturbed vein patterns (Figure 1C). Further, *nas124* and *nas234* contain respectively 6.5% and 27% of the NA concentration compared to WT (Figure 1D). It is expected that residual NA detected in *nas124* comes from NAS3 lowly expressed in roots and leaves while NA detected in *nas234* comes from NAS1 activity both strongly expressed in roots when compared to leaves (Figure S1C).

### *Loss of nucleolar iron in nas124*

NA is a central ligand for intracellular iron (Bauer *et al.*, 2004; Klatte *et al.*, 2009). Therefore we determined the impact of reduced NA content on the accumulation of nucleolar iron in *nas124* and *nas234* plants. We performed Perls associated with diaminobenzidine (Perls/DAB) staining (Figure 2 and Supplementary Fig. S2A). The Perls/DAB staining detected iron in the nucleolus of WT and *nas234* mesophyll cells (black staining, upper and lower panels). However, no iron was detected in *nas124* nucleoli (middle panel). Similarly, Perls/DAB staining of roots cells detected iron in WT and *nas234* nucleoli but not in *nas124* nucleoli (Supplementary Fig. S3). We also observed that iron formed aggregates in the xylem vessels of *nas124,* that might correspond to iron-ferritin complexes or Fe precipitates of unknown origin (Supplementary Fig. S2). Besides, increased ferritin protein levels were detected in *nas124* (Supplementary Fig. S2B). All together, these results show that simultaneous disruption of *NAS1*, *2* and *4* genes and decreased NA amount provoke loss of nucleolar iron.

### *Absence of iron in nas124 nucleoli does not change nucleolar/nuclear redox state*

As ferrous ion ($Fe^{2+}$) is highly reacting with $H_2O_2$ to produce hydroxide ($OH^-$) and hydroxyl ($OH^\cdot$) radicals through Fenton reactions, we reasoned that the contrasted iron accumulation in the nucleolus between WT and *nas124* plants might change the redox state of the nucleolus or the

surrounding nucleoplasm. To monitor the nuclear redox state in WT and *nas124* plants, we used the redox sensor roGFP2 (Figure 3A), in which the roGFP2 is fused to the glutaredoxin GRX1 (Gutscher *et al.*, 2008) and indicates the redox state by excitation at different wavelengths. This construct is expressed in the cytosol and the nuclear compartments but is excluded from the nucleolus (Figure 3B). To monitor the redox state also in the nucleolus, we fused the GRX1-roGFP2 with the GAR domain of the Fibrillarin2 (Fib2) protein, which targets the protein to the nucleolus (Barneche *et al.*, 2000) and allows documenting the redox state in the nucleolus and in the nucleoplasm (Figure 3B). The system was calibrated with $H_2O_2$ and DTT, respectively, to fully oxidize or reduce roGFP and Fib2-roGFP2, and confirmed that both sensors are similarly responsive to the redox environment (Figure 3C-E). When comparing the fluorescence ratio (405/488 nm) in WT and *nas124* plants, we observed that the ratio is close to the ratio measured under DTT treatment, suggesting that in both genetic backgrounds, the redox sensor is fully reduced in the nucleolus and the nucleus (Figure 3D-E). Therefore, we conclude that different iron contents in WT and *nas124* nucleoli do not impact the nucleolar or the nuclear redox state.

Furthermore, we measured ROS accumulation *in planta* by staining *nas124* plants with 3,3'-diaminobenzidine (DAB) and nitro blue tetrazolium (NBT) that react with $H_2O_2$ and $O_2^{\cdot-}$, respectively. Similar staining was found in *nas124* and WT plants (Supplementary Fig. S4A). Major ROS detoxification enzymes, catalases and ascorbate peroxidases, had also similar activities in WT and *nas124* plants (Supplementary Fig. S4B). In summary, *nas124* mutants do not experience oxidative stress due to perturbed iron distribution

## *Transcriptome analysis of nas124 plants*

Disruption of nucleolar organization affects nuclear gene expression in *A. thaliana* (Pontvianne *et al.*, 2016). To investigate the impact of reduced nucleolar iron and/or decreased NA on global gene expression, we performed RNAseq analysis of WT and *nas124* plants, with good correlation between two replicates (Figure 4 and Supplementary Fig. S5A and Table S1A). We identified 60 differentially expressed (DE) genes with FDR inferior to 5%. Among them were 28 up-regulated genes with fold-change (log2) values (*nas124*/WT) $\geq 2$, and 32 down-regulated genes with fold-change (log2) values $\leq 0.5$ (Figure 4A and Supplementary Table S1B). The most down-regulated gene was *NAS1* (-8.1 fold) and the most up-regulated gene encodes for hypothetical protein At1g64795 (8.1 fold). The *NAS2* and *NAS4* genes did not appear among the 60 DE genes, nevertheless decreased number of *NAS2* and *NAS4* reads (-2.2 and -1.6 fold respectively) and slightly increased number of NAS3 reads (1.3 fold) are observed in *nas124* plants (Figure 4B and Supplementary Table S1). Down regulated genes other than the *NAS* are the iron metabolism-related gene *FERRETIN 1* (At5g01600) and defense or pathogen response genes, including the S-adenosyl-L-methionine-dependent methyltransferase superfamily protein gene (At2g32160). Among the up regulated are detected *OLIGOPEPTIDE TRANSPORTER*, *OPT3* (At4g16370), *IRON REGULATED TRANSPORTER 3, IRT3* (At1g60960) and *IRONMAN 2* (At1g47395) (Supplementary Table S1B). Furthermore, a Gene Ontology (GO-PANTHER) analysis of protein classes highlighted two categories: “metabolism interconversion enzymes” (6 DE genes) and “transporters” (6 DE genes), whilst the GO-Slim molecular function and biological processes highlight the categories “catalytic activity” (12 DE genes) “/binding” (8 DE genes), and “cellular processes” (13 DE genes), respectively (Figure 4C and Supplementary Table S2). Lastly, further analysis to determine deregulation of non-coding RNA did not reveal significant transcriptomic variations of small (snoRNA, snRNA, tRNA) or long non-coding RNAs in *nas124* plants

(Supplementary Fig. S5B). Taken together, RNAseq analysis shows that simultaneous disruption of *NAS1*, *NAS2,* and *NAS4* affects expression of genes involved in metal metabolism and/or transport, and accumulation of transcripts associated to plant defense or pathogen response.

## *Functional organization of nas124 nucleoli*

We performed Transmission Electron Microscopy (TEM) analysis to investigate if reduced amounts of nucleolar iron in *nas124* plants could impact nucleolar structural and/or functional organization (Figure 5). In the nucleolus, three major functional structures are observed: Fibrillar centers (FC) where transcriptionally active 45S rDNA localizes, Dense Fibrillar Components (DFC), the place of primary rRNA processing events, and the Granular Component (GC), mainly composed of pre-ribosome particles. Transcription of rDNA by RNA Pol I occurs at the interface of FC and DFC.

In plant cells, there are two types of FCs: homogeneous FCs, many and small and associated to active nucleoli, and heterogeneous FCs, fewer and larger, associated with low rates of nucleolar activity (Saez-Vasquez and Medina, 2008). To address this issue in *nas124*, we performed TEM of nucleoli from 5, 10 and 15 day-old WT and *nas124* plants. Then we measured nucleoli periphery and determined the number of FC per nucleolus (left and right graphs respectively in Figure 5). In 5 day-old plants (red bars), nucleoli from both genotypes are larger than nucleoli from 10 (green bars) and 15 day-old (blue bars) plants. Also 5 day-old plant nucleoli from WT and *nas124* are similar in size and shape, containing between 5 to 30 FC. In 10 days-old plants, WT and *nas124* nucleoli also have similar size and functional (FC, DFC and GC) organization. However, *nas124* nucleoli contain around twice more FC structures than WT nucleoli. Likewise, nucleoli from 15 days-old WT and *nas124* plants display similar sizes, but a higher number of FC is observed in *nas124* (between 12 and 30 FC) than in WT (≤15 FC). Taken together, the TEM results suggest that *nas124* nucleoli are more active compared to WT nucleoli.

## *NOR organization and expression in nas124*

The genome of *Arabidopsis thaliana* Col-0 contains around 1,500 copies of 45S rDNA units per diploid genome (Layat *et al.*, 2012; Mohannath *et al.*, 2016; Saez-Vasquez and Gadal, 2010). They localize in the nucleolar organizer regions (NORs) from chromosomes 2 and 4 (NOR2 and NOR4) (Copenhaver and Pikaard, 1996a, b), however, only rDNA (VAR2 and 3) from NOR4 is transcribed in most plant organs. The rDNA (VAR1) from NOR2 is repressed by epigenetic mechanisms and expressed mainly early during seed germination and in specific mutant plants with nucleolar disorganization (Pontvianne *et al.*, 2010), lower copy numbers (Pontvianne *et al.*, 2013), or altered proportion of rDNA variants (Durut *et al.*, 2014).

Active NORs are associated to the nucleolus while inactive NORs remain at the nuclear periphery (Sáez-Vásquez and Delseny, 2019). To examine nucleolus association/dissociation of NORs in *nas124* plants, we performed Fluorescence *In Situ* Hybridization (FISH) with a probe homologous to the 45S rDNA (Figure 6A). In WT nuclei, the FISH probe detects a single and strong signal (active NOR4) associated to the nucleolus while two weak signals close to the nuclear border reflect the non-associated, inactive NOR2. In contrast, in *nas124* nuclei, the FISH probe detects 3-4 strong signals associated to the nucleolus. The analysis based on 32 WT and 18 *nas124* nuclei revealed around 2-fold more nucleolus-associated and around 3-fold less of non-associated signals in *nas124* nuclei

compared to WT. This increased association between the nucleolus and NOR2 indicates transcriptional activation of this usually silent rDNA locus.

To verify expression of NOR2 and NOR4 in *nas124* plants, we performed RT-PCR analysis using specific primers that amplify 3'ETS (External Transcribed Spacer) rDNA from NOR2 (*VAR1*) and/or from NOR4 (*VAR2* and *3*) (Pontvianne *et al.*, 2010). RT-PCR amplification of the 3'ETS generated specific product sizes for each rRNA gene variant (Figure 6B) and confirmed expression of VAR1 in *nuc1-2* plants with disrupted nucleolin 1 (NUC1), as reported (Pontvianne et al., 2010; Durut et al., 2014) and used as a positive control here. The analysis detected expression of rRNA *VAR1* in *nas124*, but not in WT or *nas234* plants. In *nas124* plants rRNA *VAR2* expression was unaltered while *VAR3* was at same point repressed. We also detected, but at lower level, expression of rRNA *VAR1* in *nas123* and *nas134*. Finally, rRNA *VAR1* is not expressed in *nas1* plants indicating that disruption of *NAS1* alone is not sufficient to induce expression of NOR2.

Furthermore, to determine rDNA copy number variations and/or organization that could have affected expression of rDNA variants, we performed PCR and qPCR using genomic DNA from WT and *nas124*, including a fourth generation of amplified homozygous mutants (Figure 6B). Except for a lower PCR signal corresponding to rDNA VAR4 observed in *nas124* compared to WT, this analysis shows no obvious differences in the ratio of rDNA variants VAR1-3 in *nas124* compared to WT plants. Similarly, RT-qPCR of ITS1 (Internal Transcribed Spacer 1), 18S, 5.8S and 25S rDNA sequences excluded significant differences in the total copy number of rDNA in the *nas124*, from 1st to 4th generation.

Transcriptionally active rDNA is hypomethylated and associated to acetylated (H3Ac and H4Ac) or dimethylated histone H3 at lysine 4 (H3K4me2), while inactive rDNA is hypermethylated and associated to dimethylated histone H3 at lysine 9 (H3K9me2) (Earley *et al.*, 2010; Espada *et al.*, 2007; Probst *et al.*, 2004). Therefore, we analyzed epigenetic state of 45S rDNA in *nas124* plants. We performed bisulfite analysis of promoter and 5'ETS rDNA (-315 to +243) sequences (Figure 6C). Notably, CG sites are more present downstream of TIS/+1 (Transcription Initiation Site at +1) whereas CHG and CHH sites are enriched upstream of TIS/+1. The bisulfite analysis revealed a slight hypermethylation in *nas124* at specific CHG (blue bars) and CHH (green bars) sites in the 5'ETS, while the CG methylation (red bars) in *nas124* remains similar to WT. Notably, in the promoter sequence, there is higher CHG and CHH methylation in *nas124* plants compared to WT. Silencing of 45S rRNA genes involve long non-coding RNA (Schmitz *et al.*, 2010) or small interfering RNA (siRNA) that direct specific DNA methylation (Costa-Nunes *et al.*, 2010). Northern blot experiments did not revealed significant differences in the accumulation of promoter siRNA 45S and siR759 or IGS rRNA sequences (Supplementary Fig. S6).

To determine if the CHG and CHH hypermethylation is specific for either *VAR1,* and/or *VAR2,* and/or *VAR3,* we performed bisulfite analysis of the 3'ETS rDNA region (Supplementary Fig. S7). In contrast to promoter and 5'ETS regions, CG, CHG and CHH sites are more equally distributed in the 3'ETS of all rDNA variants. The bisulfite analysis did not reveal significant differences in the methylation state between rDNA variants from *nas124* and WT plants. Only one CG site at position 44 in *VAR1* was hypomethylated in *nas124*.

We also examined histone marks by Chromatin Immuno-Precipitation (ChIP) followed by qPCR analysis (Supplementary Fig. S8). Primers matching mature 25S and non-coding (IGS, 5'ETS and

3'ETS) rDNA sequences did not detect changes of neither active (H3Ac and H3K4me2) nor inactive (H3K9me2) histone marks in *nas124* compared to WT plants.

Together these analyses revealed that among the epigenetic parameters investigated, changes in DNA methylation at rDNA promoter sequences are most evident with expression of rDNA from NOR2 in the *nas124* mutant. In contrast, in the *nas234* mutant we do not observe NOR2 activity and/or nucleolus association or neither epigenetic changes (Supplementary Fig. S9).

### *RNA methylation in nas124 and nas234 plants*

rRNA is modified concomitantly or immediately after RNA pol I transcription. Reported rRNA modifications include sugar and base methylation and/or acetylation, and serve to stabilize structures of the rRNA scaffold and ensure efficiency and accuracy of translation (Sharma and Lafontaine, 2015; Sloan *et al.*, 2017). Since S-adenosyl-methionine (SAM) moieties used by NAS enzymes to synthetise NA are also donor in methylation reactions, including methylation of DNA, RNA and proteins (Figure 1), we questioned whether reduced NAS activity in the *nas124* and *nas234* plants might impact availability of SAM and subsequently methylation of coding and non-coding RNAs. Here, we studied the impact of NAS reduction (in *nas124* and *nas234*) and/or the expression of rRNA from NOR2 (in *nas124*) on RNA base modifications and on 2'-*O*-methylation, the most abundant rRNA modification (Azevedo-Favory *et al.*, 2021; Wu *et al.*, 2021).

We performed MRM methodology in mass spectrometry to analyze 18 different RNA base modifications (Figure 7 and Supplementary Fig. S10), including $m^1A$, $m^5C$, $m^7G$, $m^3A$ and $ac^4C$ identified in rRNA from yeast and animal cells (Sharma and Lafontaine, 2015; Sloan *et al.*, 2017). The foremost observation is a significant (≤ 0.05) increase of methylation of $m^1A$, $m^1G$, $m^{2,7,7}G$, $m^3C$, $m^5C$, $m^7G$, and also $ac^4C$ in *nas124*. No decreased methylation of specific RNA modifications was observed in *nas124*. In contrast, methylation of $m^1A$, $m^3C$, $m^5C$, $m^7G$, $m^{2,2}G$, $m^3U$, $mcm^5s^2U/U$, $ncm^5U/U$ was decreased in *nas234* while methylation of $m^{2,7,7}G$ and $m^6A$ increased. No significant changes were detected for I, $m^2G$, $m^6Am$, $m_2^6A$, $oxo^8G$ and/or pseudouridylation (Psi) in *nas124* or *nas234* (Figure 7, Supplementary Table S3).

We performed RiboMethSeq analysis to determine 2'-*O*-methylation (2'-*O*-Me) profiles of 18S, 5.8S and 25S rRNA in *nas124* and *nas234* compared to WT plants. No significant changes were detected in *nas124* or *nas234* plants (Supplementary Fig. S10A and Table S4).

Together, these analyses reveal specific RNA base methylation changes in *nas124* and *nas234*. Notably RNA base methylation changes detected in *nas124* are opposite to, or are not affected in *nas234*.

## Discussion

The *nas124* and *nas234* plants described here each have a reduced concentration of NA, however specific cellular and molecular features were detected in these plant mutants. Under standard growth conditions, a reduced concentration of NA does not have an evident impact in *nas124* or *nas234* plant growth or development phenotypes, excepted for mild disturbed vein patterns in cotyledons in both genotypes and chloronerva-like phenotypes in primary leaves in *nas124* (Figure

1). A leaf chlorosis was also observed in the fertile and quadruple mutant *nas4x-1*. However, this chlorosis was minor at vegetative stage and intensified at the reproductive stage (Klatte *et al.*, 2009).

Nevertheless, the most outstanding observation is that only *nas124* contains low or undetectable iron in the nucleolus (Figure 2 and Supplementary Fig. S2 and S3). We cannot yet explain the chloronerva-like and low nucleolar iron phenotypes in *nas124,* which does not occur in *nas234* plants. The lower amount of total NA in *nas124* and the lack of NAS activity in roots might have an impact in iron transport from tissue to tissue, cell to cell and at last to the nucleolus. However, inhibition of iron uptake or increased iron availability did not affect *nas124* growth (root phenotype) compared to WT plants; neither alterations of the media composition (MS and/or sugar) changed chlorosis in *nas124* (Supplementary Fig. S11).

Transcriptome analysis does not explain phenotypes of *nas124* plants (Figure 4 and Supplementary Fig. S5). However, mRNA transcripts encoding proteins involved in iron metabolism or transport are de-regulated in *nas124* plants, indicating a disturbed sensing of iron availability status in these plants. In addition, variations of transcripts associated with plant defense or pathogen response indicate that *nas124* might be also sensitive to biotic stresses. This in agreement with reported role of iron in plant pathogenesis response (reviewed in (Liu *et al.*, 2021).

How reduced NA inhibits nucleolar accumulation of iron in *nas124*, but not in *nas234*, remains an open question. However, the finding of low or undetectable iron in the nucleolus in *nas124* allowed us to address the role of nucleolar iron in plants.

The functional and structural organization of the nucleolus is linked to ribosome biogenesis (Boulon *et al.*, 2010; Saez-Vasquez and Medina, 2008). In *nas124,* the lack of nucleolar iron induces increased number of FC likely due to rRNA VAR1 expression from normally silenced NOR2. It may be expected that rDNA VAR1 expression in *nas124* is a consequence of failed repression rather than activation of NOR2. This is in agreement with steady rDNA *VAR1* expression in *nas124* early during seedling establishment (Supplementary Fig. S12). Indeed, in early states of seedling establishment, NOR2 and NOR4 are both expressed in WT plants. Later, NOR2 becomes progressively silenced (Benoit *et al.*, 2013; Durut *et al.*, 2014; Earley *et al.*, 2010). Expression of NOR2 and low nucleolar iron and the presence of aggregates in the xylem vessels is also observed *nuc1-2* plants (Supplementary Fig. S2). However, in contrast to *nas124,* disruption of NUC1 also induced nucleolus disorganisation, chromatin de-condensation and rDNA hypomethylation (Pontvianne *et al.*, 2010; Pontvianne *et al.*, 2007), indicating that loss of nucleolar iron and NOR2 expression are triggered by different mechanisms.

Expression of rRNA *VAR1* is associated with rDNA CpG hypomethylation, rDNA copy number or ratio, rDNA chromatin decondensation and/or modifications of histone marks (Durut *et al.*, 2014; Earley *et al.*, 2010; Mozgova *et al.*, 2010; Pontvianne *et al.*, 2010; Pontvianne *et al.*, 2012; Pontvianne *et al.*, 2013). None of these features are affected in *nas124* (Figure 6). In contrast, CHG and CHH methylation on the rDNA promoter are increased in *nas124*. This is unexpected, as increased DNA methylation is generally correlated with gene repression (Earley *et al.*, 2006; Espada *et al.*, 2007; Probst *et al.*, 2004). In this context, the conserved iron-sulfur cluster assembly protein MET18, could play a key role. Indeed, in Arabidopsis *MET18* gene disruption causes DNA hypermethylation in particular in the CHH context (Wang *et al.*, 2016). Interestingly, similarly to *nas124* the rRNA *VAR1* accumulates in *met18* plants (Supplementary Fig. S13). Therefore, in *nas124*, lacks of nucleolar iron might inhibit MET18 causing CHH hypermethylation of rDNA.

In animal cells there is a subset of rRNA genes that are transcriptionally inactive but are poised for transcription activation. Such poised rDNA promoters are unmethylated and are marked by both euchromatic and heterochromatic histone modifications (Grummt and Langst, 2013; Xie *et al.*, 2012). Therefore we can speculate that hypermethylation *in nas124* happens on "poised rDNA promoters" rather than on transcriptionally active rDNA. Furthermore, higher numbers of FC in *nas124*, is a likely consequence of nucleolar association of NOR2 and an increased number of transcribed rRNA genes. However, we predict a low RNA pol I transcription activity on these rRNA genes since accumulation of rRNA precursors and/or mature 18S, 5.8S and 25S rRNA in *nas124* is similar to WT and *nas234* plants (Supplementary Fig. S14). Controlling rRNA synthesis by modulating RNA pol I loading on rDNA and activity has been reported in yeast and animal cells (Darriere *et al.*, 2019; French *et al.*, 2003; Goodfellow and Zomerdijk, 2013).

NAS enzymes use SAM to produce NA (Figure 1) and it is not excluded that reduced rates of NA synthesis in *nas124* and *nas234* might fine-tune SAM availability and subsequently affect methylation of RNA, DNA and/or proteins. Remarkably, in contrast to the lack of nucleolar iron and NOR2 gene expression detected in *nas124,* RNA methylation modifications are impacted in both *nas124* and *nas234* (Figure 7). However, the specific and contrasting changes of RNA modifications levels in *nas124* and *nas234* are intriguing. For instance, whereas increased level of RNA modifications (including $m^1A$, $m^5C$, $m^7G$) could be correlated with a differential rRNA gene expression in *nas124*, this is not the case for decreased level of these same RNA modifications in *nas234.* The identification of RNA targets differentially methylated in *nas124* and *nas124* requires further investigation. However, detected modifications $m^1A$, $m^5C$, $m^7G$ and $ac^4C$ are likely associated with rRNA because they are the most abundant cellular RNAs and the first to be detected by LC-MSMS. These modifications occur co-transcriptionally in the nucleolus (Sharma and Lafontaine, 2015; Sloan *et al.*, 2017), and it is tempting to propose that lack of nucleolar iron might affect the activity of iron–sulfur (Fe/S) protein factors involved in depositing RNA modifications. Notably, several rRNA modifications are introduced by RNA modifying enzymes containing (Fe/S) clusters (Kimura and Suzuki, 2015). However, to our knowledge, rRNA modifying enzymes containing (Fe/S) clusters have not yet been reported in plants.

Redox-active iron (Fe2+, iron (II)) has a potential to produce a highly reactive $^{\cdot}OH$ radicals by Fenton reaction when it meets hydrogen peroxide (Smethurst and Shcherbik, 2021). However, nuclear/nucleolar redox state seems unaffected in *nas124*, suggesting that nucleolar iron accumulating in wild-type plants is likely unavailable for Fenton reactions. We did not observe more pronounced ROS accumulation, indicating that *nas124* does not experience oxidative stress due to perturbed cellular/or subcellular iron distribution (Figure 3 and Supplementary Fig. S4). Nevertheless, it is of particular interest to highlight that the ribosome, which generally depends on $Mg^{2+}$, might also contain several $Fe^{2+}$ at specific sites (Smethurst *et al.*, 2020). Therefore, further characterization of *nas124* plants should help us to understand the role of iron in ribosome assembly and/or activity specifically under oxidative conditions.

## Figure Legends

**Figure 1:** Nicotianamine synthesis and nas124 and nas234 plants A) aThe synthesis of NA by NAS (NicotiAnamine Synthase) from three molecules of SAM includes two carboxypropyl group transfers and one azetidine ring formation, with three molecules of 50-methylthioadenisine (50-MTA) released. bNA chelates metal ions including iron. cSAM is also a methyl donor in methylation reactions including methylation of DNA, RNA and proteins B) WT, nas124 and nas234 plants grown for 12 days in vitro. Bar = 2.5 mm C) Cleared cotyledon leaves of WT and nas124 and nas234 plants, viewed under dark-field illumination. D) Nicotianamine (NA) content in 15 days-old in vitro grown WT, nas124 and nas234 plants. Scale bar = 0.4 mm. Data are means ±SE of n=3 independent pools of 3 plants each, * indicate statistical difference with Wilcoxon test, P<0.1.

**Figure 2: Nucleolar iron in *nas124* and *nas234*** Leaf sections showing mesophyll cells from 15 days-old WT (A and B), *nas124* (C and D) and *nas234* (E and F) plants grown *in vitro* were stained with Perls/DAB. Arrows indicate nucleolar iron in WT and *nas234*. Scale bars = 40 µm for panel a, c and e and 20 µm for panels b, d and f.

**Figure 3: *In vivo* monitoring of nucleolar/nuclear redox state in *nas124* A)** Gene structure of the roGFP2 constructs used to transform WT and *nas124* plants. Both constructs are under the control of the 35S-CaMV promoter. In Fib2-roGFP2, GRX1 is fused to roGFP2 as in roGFP2, but the GAR domain (1-73 N-term amino acids) of Fib2 is additionally fused to GRX1-roGFP2. Scale bars = 10 µm **B**) Confocal images of nuclei of WT cotyledons expressing roGFP2 or Fib2-roGFP2. RoGFP2 was excited at 488 nm or 405 nm to monitor the reduced or oxidized forms, respectively. Arrows indicate the nucleolus. **C)** Steady state ratio images of WT or *nas124* plants expressing roGFP2 or Fib2-roGFP2 and calculated as the 405/488 nm fluorescence. To fully reduce or oxidize the sensor, seedlings were immersed in 10 mM DTT or 100 mM $H_2O_2$, respectively. Control samples were immersed in MS/2 liquid medium only. False colors indicate the fluorescence ratio on a scale from blue (reduced) to red (oxidized). Scale bars = 10 µm. White circles indicate the location of the nucleolus. **D-E)** Fluorescence ratio of roGFP2 (D) and Fib2-roGFP2 (E) calculated from ratio images. Ratios were calculated from 6 to 16 nuclei per sample. Asterisks indicate a significant difference calculated by Student's t-test (* $p \leq 0.05$, ** $p \leq 0.01$, and *** $p \leq 0.001$, ns $p > 0.05$).

**Figure 4: Transcriptomic analysis of *nas124* A)** Heat map of 60 DE genes in 15 days-old *in vitro* grown *nas124* compared to WT plants. The color key, histogram and values are shown. Down- and up-regulated genes are in green and red, respectively **B)** Graph of normalized reads (rpkm) in WT and *nas124* plants for *NAS1* (At5g04950), *NAS2* (At5g56080), *NAS3* (At1g09240) and *NAS4* (At1g09240) transcripts. Graphs and plots were generated using RStudio, Ri 386 version 4.1.1. **C)** Gene Ontology (GO) analysis for -protein classes, -Slim molecular function and -Slim Biological Processes.

**Figure 5: Nucleolus organization in *nas124*. Top,** Transmission Electron Microscopy (TEM) on root cells from 10 days-old WT and *nas124* plants grown *in vitro*. The Fibrillar Centers (FC) are surrounded by the Dense Fibrillar Component (DFC, pointed by white arrows) and embedded in the Granular Component (GC). Scale bar = 500 nm. **Bottom**, boxplot graphs of nucleoli periphery (Left) and number of FC structures per nucleolus (Right) in 5 (red), 10 (green) and 15 (blue) days-old root cells.

The dots indicate the outlier samples. 28 (5 days-old), 13 (10 days-old) and 46 (15 days-old) WT nucleoli and 35 (5 days-old), 19 (10 days-old) and 16 (15 days-old) *nas124* nucleoli were analyzed. Asterisks indicate a significant difference calculated by Student's t-test: ns > 0.05, * ≤0.05, ** ≤0.01 *** ≤0.001 and **** ≤0.001.

**Figure 6: NOR expression in *nas124* A)** Fluorescent *In Situ* Hybridization (FISH) analysis of 45S rDNA performed on leaf cells from 21 days-old WT and *nas124* plants grown on soil. 45S-labelled probes hybridized to NOR2 and NOR4 (red signals). DNA in the nucleoplasm is stained in blue with DAPI and the black area in the nucleus corresponds to the nucleolus that is not stained because the rDNA chromatin is decondensed and too thin to be stained by DAPI (Pontvianne *et al.*, 2016a). Scale bars = 5 µm. The histogram shows the number of 45S FISH signals in 32 WT and 18 *nas124* cells. Green bars show the number of nucleolus associated signals and the purple bars nucleolus non associated signals **B) Top panels,** RT-PCR to detect 45S pre-rRNA variants in leaves from 21 days-old WT (lane 1), *nuc1-2* (lane 2), *nas1* (lane 3), *nas124* (lane 4 and 9) *nas234* (lane 5 and 8), *nas123* (lane 7) and *nas134* (lane 10) plants grown on soil. Amplification of 18S (lanes 1-5) and EF1-alpha (lanes 7-10) RNA transcripts was performed to verify similar amount of RNA in each sample. Amplification of genomic DNA (lane 6) shows up to four rDNA variants in *Arabidopsis thaliana* Col-0 plants; **Bottom panels,** PCR (left) analysis of 3'ETS rDNA in WT (lane 1) and *nas124* (lane 2) plants and RT-qPCR (right) of 18S (red), Internal Transcribed Spacer 1 (ITS1a, green and ITS1b, blue), 25S (orange) and 5.8S (purple) rDNA sequences in WT and *nas124* sibling (G1 and G4) **C)** Bisulfite analysis of promoter/5'ETS (from -315 to +243) rDNA sequences from WT and *nas124* plants. The graph bars show CG (red), CHG (blue) and CHH (green) methylation level at different position in the rDNA. The tiny dark stars over the graph bars indicate sites with significant (*p* values ≤0.05) difference of methylation rate between WT and *nas124* for each position **D)** The scheme of a 45S rDNA unit shows position of primers used in bisulfite sequencing analysis (o112/o113), to amplify rDNA for FISH probe (o145/o146), to detect 3'ETS (o108/o109) by PCR and 18S (o1257/o1258), ITS1 (o1262/o1263 and o1259/o1261), 5.8S (o1266/o1267) and 25S (o1264/o1265) by qPCR.

**Figure 7: RNA modifications in *nas124* and *nas234*.** Graphs show ratio of $ac^4C$/C, I/U, $m^1A$/U, $m^1G$/G, $m^{2,2,7}G$/G, $m^7G$/G, $m^{2,2}G$/G, $m^2G$/G, $m^3C$/C, $m^3U$/U, $m^5C$/C, $m_2^6A$/U, $m^6A$/U, $m^6Am$/U, $mcm^5s^2U$/U, $ncm^5U$/U, $oxo^8G$/G and Psi/U detected by LC-MRM method in WT and *nas124*. *p* values are indicated for each methylated/non-methylated nucleotide ratio. Asterisks indicate a significant difference calculated by Student's t-test: ns > 0.05, * ≤0.05, ** ≤0.01 and ****p* ≤0.001. Statistical difference with Wilcoxon test, *p* ≤0.1 are provided for $m^{6,6}A$/U, $mcm^5s^2U$/U, $ncm^5U$/U.

## Acknowledgments

The authors thank Michel Delseny and Ortrun Mittelsten Scheid for critical reading of the manuscript and Hervé Moreau for facilitating access to the BioPIC platform. We also thanks Tom Roscoe for comments and correction of the English; Karl Ravet for antibodies against Arabidopsis ferritin and S. Brando and M. Laudie for technical assistance.

## Author contributions

CM, CR, WL, FP, TD, AB, EJ, MLE, ADB, AW, JPR performed the experiments. MCC, performed bioinformatics analysis, MGMA obtained *nas* triple mutant lines, AA., CH., and AD performed LC-MRM and VM and YM performed RiboMetSeq. SBG provided technical assistance. SM, CC supervised experiments. JSV, CM and JPR analyzed data and wrote the manuscript. All authors approved the final manuscript.

## Conflict of Interest

The authors declare that they have no conflict of interest in relation to this work

## Funding

This work was supported by the CNRS, the UPVD (fellowships to CM), by grants ANR SUBCELIF 087217 and MetRibo 210877 and RoxRNase 210880 and Labex AGRO (under I-Site Muse framework) coordinated by the Agropolis Fondation (grant no. Flagship Project 1802-002 – CalClim). This study is set within the framework of the “Laboratoires d’Excellences (LABEX)” TULIP (ANR-10-LABX-41) and of the "Ecole Universitaire de Recherche (EUR)" TULP-GS (ANR-18-EURE-00019).

## Data availability

All data supporting the findings of this study are available within the paper and within its supplementary materials published online.

## References


**Anders S, Pyl PT, Huber W**. 2015. HTSeq--a Python framework to work with high-throughput sequencing data. Bioinformatics **31**, 166-169.

**Azevedo-Favory J, Gaspin C, Ayadi L, Montacie C, Marchand V, Jobet E, Rompais M, Carapito C, Motorin Y, Saez-Vasquez J**. 2021. Mapping rRNA 2'-O-methylations and identification of C/D snoRNAs in Arabidopsis thaliana plants. RNA Biology **18**, 1760-1777.

**Barneche F, Steinmetz F, Echeverria M**. 2000. Fibrillarin genes encode both a conserved nucleolar protein and a novel small nucleolar RNA involved in ribosomal RNA methylation in Arabidopsis thaliana. Journal of Biological Chemistry **275**, 27212-27220.

**Bauer P, Thiel T, Klatte M, Bereczky Z, Brumbarova T, Hell R, Grosse I**. 2004. Analysis of sequence, map position, and gene expression reveals conserved essential genes for iron uptake in Arabidopsis and tomato. Plant Physiology **136**, 4169-4183.

**Benoit M, Layat E, Tourmente S, Probst AV**. 2013. Heterochromatin dynamics during developmental transitions in Arabidopsis - a focus on ribosomal DNA loci. Gene **526**, 39-45.

**Boulon S, Westman BJ, Hutten S, Boisvert FM, Lamond AI**. 2010. The nucleolus under stress. Molecular Cell **40**, 216-227.

**Bray MS, Lenz TK, Haynes JW, Bowman JC, Petrov AS, Reddi AR, Hud NV, Williams LD, Glass JB**. 2018. Multiple prebiotic metals mediate translation. Proceedings of the National Academy of Sciences of the United States of America **115**, 12164-12169.

**Briat JF, Dubos C, Gaymard F**. 2015. Iron nutrition, biomass production, and plant product quality. Trends in Plant Science **20**, 33-40.

**Copenhaver GP, Pikaard CS**. 1996a. RFLP and physical mapping with an rDNA-specific endonuclease reveals that nucleolus organizer regions of Arabidopsis thaliana adjoin the telomeres on chromosomes 2 and 4. The Plant Journal **9**, 259-272.

**Copenhaver GP, Pikaard CS**. 1996b. Two-dimensional RFLP analyses reveal megabase-sized clusters of rRNA gene variants in Arabidopsis thaliana, suggesting local spreading of variants as the mode for gene homogenization during concerted evolution. The Plant Journal **9**, 273-282.

**Costa-Nunes P, Pontes O, Preuss SB, Pikaard CS**. 2010. Extra views on RNA-dependent DNA methylation and MBD6-dependent heterochromatin formation in nucleolar dominance. Nucleus **1**, 254-259.

**Curie C, Briat JF**. 2003. Iron transport and signaling in plants. Annual Review of Plant Biology **54**, 183-206.

**Darriere T, Pilsl M, Sarthou MK, Chauvier A, Genty T, Audibert S, Dez C, Leger-Silvestre I, Normand C, Henras AK, Kwapisz M, Calvo O, Fernandez-Tornero C, Tschochner H, Gadal O**. 2019. Genetic analyses led to the discovery of a super-active mutant of the RNA polymerase I. PLoS Genetics **15**, e1008157.

**Durut N, Abou-Ellail M, Pontvianne F, Das S, Kojima H, Ukai S, de Bures A, Comella P, Nidelet S, Rialle S, Merret R, Echeverria M, Bouvet P, Nakamura K, Saez-Vasquez J**. 2014. A duplicated NUCLEOLIN gene with antagonistic activity is required for chromatin organization of silent 45S rDNA in Arabidopsis. The Plant Cell **26**, 1330-1344.

**Earley K, Lawrence RJ, Pontes O, Reuther R, Enciso AJ, Silva M, Neves N, Gross M, Viegas W, Pikaard CS**. 2006. Erasure of histone acetylation by Arabidopsis HDA6 mediates large-scale gene silencing in nucleolar dominance. Genes & development **20**, 1283-1293. Epub 2006 Apr 1228.

**Earley KW, Pontvianne F, Wierzbicki AT, Blevins T, Tucker S, Costa-Nunes P, Pontes O, Pikaard CS**. 2010. Mechanisms of HDA6-mediated rRNA gene silencing: suppression of

intergenic Pol II transcription and differential effects on maintenance versus siRNA-directed cytosine methylation. Genes & development **24**, 1119-1132.
**Espada J, Ballestar E, Santoro R, Fraga MF, Villar-Garea A, Nemeth A, Lopez-Serra L, Ropero S, Aranda A, Orozco H, Moreno V, Juarranz A, Stockert JC, Langst G, Grummt I, Bickmore W, Esteller M**. 2007. Epigenetic disruption of ribosomal RNA genes and nucleolar architecture in DNA methyltransferase 1 (Dnmt1) deficient cells. Nucleic Acids Research **35**, 2191-2198.
**French SL, Osheim YN, Cioci F, Nomura M, Beyer AL**. 2003. In exponentially growing Saccharomyces cerevisiae cells, rRNA synthesis is determined by the summed RNA polymerase I loading rate rather than by the number of active genes. Molecular and Cellular Biology **23**, 1558-1568.
**Goodfellow SJ, Zomerdijk JC**. 2013. Basic mechanisms in RNA polymerase I transcription of the ribosomal RNA genes. Subcellular Biochemistry **61**, 211-236.
**Grummt I, Langst G**. 2013. Epigenetic control of RNA polymerase I transcription in mammalian cells. Biochimica et Biophysica Acta **1829**, 393-404.
**Gutscher M, Pauleau AL, Marty L, Brach T, Wabnitz GH, Samstag Y, Meyer AJ, Dick TP**. 2008. Real-time imaging of the intracellular glutathione redox potential. Nat Methods **5**, 553-559.
**Heeney MM, Finberg KE**. 2014. Iron-refractory iron deficiency anemia (IRIDA). Hematology/Oncology Clinics of North America **28**, 637-652, v.
**Henle ES, Han Z, Tang N, Rai P, Luo Y, Linn S**. 1999. Sequence-specific DNA cleavage by Fe2+-mediated fenton reactions has possible biological implications. Journal of Biological Chemistry **274**, 962-971.
**Henle ES, Luo Y, Gassmann W, Linn S**. 1996. Oxidative damage to DNA constituents by iron-mediated fenton reactions. The deoxyguanosine family. Journal of Biological Chemistry **271**, 21177-21186.
**Hernandez-Verdun D, Roussel P, Thiry M, Sirri V, Lafontaine DL**. 2010. The nucleolus: structure/function relationship in RNA metabolism. Wiley Interdisciplinary Reviews: RNA **1**, 415-431.
**Honda K, Smith MA, Zhu X, Baus D, Merrick WC, Tartakoff AM, Hattier T, Harris PL, Siedlak SL, Fujioka H, Liu Q, Moreira PI, Miller FP, Nunomura A, Shimohama S, Perry G**. 2005. Ribosomal RNA in Alzheimer disease is oxidized by bound redox-active iron. Journal of Biological Chemistry **280**, 20978-20986.
**Kim D, Langmead B, Salzberg SL**. 2015. HISAT: a fast spliced aligner with low memory requirements. Nat Methods **12**, 357-360.
**Kimura S, Suzuki T**. 2015. Iron-sulfur proteins responsible for RNA modifications. Biochimica et Biophysica Acta **1853**, 1272-1283.
**Klatte M, Schuler M, Wirtz M, Fink-Straube C, Hell R, Bauer P**. 2009. The analysis of Arabidopsis nicotianamine synthase mutants reveals functions for nicotianamine in seed iron loading and iron deficiency responses. Plant Physiology **150**, 257-271.
**Kumar N, Rizek P, Jog M**. 2016. Neuroferritinopathy: Pathophysiology, Presentation, Differential Diagnoses and Management. Tremor and Other Hyperkinetic Movements **6**, 355.
**Langmead B, Salzberg SL**. 2012. Fast gapped-read alignment with Bowtie 2. Nat Methods **9**, 357-359.
**Layat E, Saez-Vasquez J, Tourmente S**. 2012. Regulation of Pol I-transcribed 45S rDNA and Pol III-transcribed 5S rDNA in arabidopsis. Plant and Cell Physiology **53**, 267-276.
**Liu Y, Kong D, Wu HL, Ling HQ**. 2021. Iron in plant-pathogen interactions. Journal of Experimental Botany **72**, 2114-2124.
**Love MI, Huber W, Anders S**. 2014. Moderated estimation of fold change and dispersion for RNA-seq data with DESeq2. Genome Biol **15**, 550.

**Marty L, Siala W, Schwarzlander M, Fricker MD, Wirtz M, Sweetlove LJ, Meyer Y, Meyer AJ, Reichheld JP, Hell R**. 2009. The NADPH-dependent thioredoxin system constitutes a functional backup for cytosolic glutathione reductase in Arabidopsis. Proceedings of the National Academy of Sciences of the United States of America **106**, 9109-9114.

**Mohannath G, Pontvianne F, Pikaard CS**. 2016. Selective nucleolus organizer inactivation in Arabidopsis is a chromosome position-effect phenomenon. Proceedings of the National Academy of Sciences of the United States of America **113**, 13426-13431.

**Mozgova I, Mokros P, Fajkus J**. 2010. Dysfunction of chromatin assembly factor 1 induces shortening of telomeres and loss of 45S rDNA in Arabidopsis thaliana. The Plant Cell **22**, 2768-2780.

**Pederson T, Powell K**. 2015. Thoru Pederson: Spotting novel roles for the nucleolus. Journal of Cell Biology **208**, 384-385.

**Pontvianne F, Abou-Ellail M, Douet J, Comella P, Matia I, Chandrasekhara C, Debures A, Blevins T, Cooke R, Medina FJ, Tourmente S, Pikaard CS, Saez-Vasquez J**. 2010. Nucleolin is required for DNA methylation state and the expression of rRNA gene variants in Arabidopsis thaliana. PLoS Genetics **6**, e1001225.

**Pontvianne F, Blevins T, Chandrasekhara C, Feng W, Stroud H, Jacobsen SE, Michaels SD, Pikaard CS**. 2012. Histone methyltransferases regulating rRNA gene dose and dosage control in Arabidopsis. Genes & development **26**, 945-957.

**Pontvianne F, Blevins T, Chandrasekhara C, Mozgova I, Hassel C, Pontes OM, Tucker S, Mokros P, Muchova V, Fajkus J, Pikaard CS**. 2013. Subnuclear partitioning of rRNA genes between the nucleolus and nucleoplasm reflects alternative epiallelic states. Genes & development **27**, 1545-1550.

**Pontvianne F, Carpentier MC, Durut N, Pavlistova V, Jaske K, Schorova S, Parrinello H, Rohmer M, Pikaard CS, Fojtova M, Fajkus J, Saez-Vasquez J**. 2016. Identification of Nucleolus-Associated Chromatin Domains Reveals a Role for the Nucleolus in 3D Organization of the A. thaliana Genome. Cell Reports **16**, 1574-1587.

**Pontvianne F, Matia I, Douet J, Tourmente S, Medina FJ, Echeverria M, Saez-Vasquez J**. 2007. Characterization of AtNUC-L1 reveals a central role of nucleolin in nucleolus organization and silencing of AtNUC-L2 gene in Arabidopsis. Molecular Biology of the Cell **18**, 369-379.

**Probst AV, Fagard M, Proux F, Mourrain P, Boutet S, Earley K, Lawrence RJ, Pikaard CS, Murfett J, Furner I, Vaucheret H, Mittelsten Scheid O**. 2004. Arabidopsis histone deacetylase HDA6 is required for maintenance of transcriptional gene silencing and determines nuclear organization of rDNA repeats. The Plant Cell **16**, 1021-1034.

**Quintana C, Bellefqih S, Laval JY, Guerquin-Kern JL, Wu TD, Avila J, Ferrer I, Arranz R, Patino C**. 2006. Study of the localization of iron, ferritin, and hemosiderin in Alzheimer's disease hippocampus by analytical microscopy at the subcellular level. Journal of Structural Biology **153**, 42-54.

**Roschzttardtz H, Fuentes I, Vásquez M, Corvalán C, León G, Gómez I, Araya A, Holuigue L, Vicente-Carbajosa J, Jordana X**. 2009. A nuclear gene encoding the iron-sulfur subunit of mitochondrial complex II is regulated by B3 domain transcription factors during seed development in Arabidopsis. Plant Physiology **150**, 84-95.

**Roschzttardtz H, Grillet L, Isaure MP, Conejero G, Ortega R, Curie C, Mari S**. 2011. Plant cell nucleolus as a hot spot for iron. Journal of Biological Chemistry **286**, 27863-27866.

**Sáez-Vásquez J, Delseny M**. 2019. Ribosome Biogenesis in Plants: from Functional 45S Ribosomal DNA Organization to Ribosome Assembly Factors. The Plant Cell **31**, 1945–1967.

**Saez-Vasquez J, Gadal O**. 2010. Genome organization and function: a view from yeast and Arabidopsis. Molecular Plant **3**, 678-690.
**Saez-Vasquez J, Medina FJ**. 2008. The plant nucleolus. In: Kader J-C, Delseny M, eds. *Botanical Research: Incorporating Advances in Plant Pathology*, Vol. 47. San Diego: Elsevier Academic Press Inc, 1-46.
**Schmitz KM, Mayer C, Postepska A, Grummt I**. 2010. Interaction of noncoding RNA with the rDNA promoter mediates recruitment of DNMT3b and silencing of rRNA genes. Genes & development **24**, 2264-2269.
**Sharma S, Lafontaine DL**. 2015. 'View From A Bridge': A New Perspective on Eukaryotic rRNA Base Modification. Trends in Biochemical Sciences **40**, 560-575.
**Sloan KE, Warda AS, Sharma S, Entian KD, Lafontaine DLJ, Bohnsack MT**. 2017. Tuning the ribosome: The influence of rRNA modification on eukaryotic ribosome biogenesis and function. RNA Biology **14**, 1138-1152.
**Smethurst DGJ, Kovalev N, McKenzie ER, Pestov DG, Shcherbik N**. 2020. Iron-mediated degradation of ribosomes under oxidative stress is attenuated by manganese. Journal of Biological Chemistry **295**, 17200-17214.
**Smethurst DGJ, Shcherbik N**. 2021. Interchangeable utilization of metals: New perspectives on the impacts of metal ions employed in ancient and extant biomolecules. Journal of Biological Chemistry **297**, 101374.
**Stepinski D**. 2014. Functional ultrastructure of the plant nucleolus. Protoplasma **251**, 1285-1306.
**Tsai RY, Pederson T**. 2014. Connecting the nucleolus to the cell cycle and human disease. The FASEB Journal **28**, 3290-3296.
**Tsekrekou M, Stratigi K, Chatzinikolaou G**. 2017. The Nucleolus: In Genome Maintenance and Repair. International Journal of Molecular Sciences **18**.
**Wang X, Li Q, Yuan W, Cao Z, Qi B, Kumar S, Li Y, Qian W**. 2016. The cytosolic Fe-S cluster assembly component MET18 is required for the full enzymatic activity of ROS1 in active DNA demethylation. Scientific Reports **6**, 26443.
**Wu S, Wang Y, Wang J, Li X, Li J, Ye K**. 2021. Profiling of RNA ribose methylation in Arabidopsis thaliana. Nucleic Acids Research **49**, 4104-4119.
**Xie W, Ling T, Zhou Y, Feng W, Zhu Q, Stunnenberg HG, Grummt I, Tao W**. 2012. The chromatin remodeling complex NuRD establishes the poised state of rRNA genes characterized by bivalent histone modifications and altered nucleosome positions. Proceedings of the National Academy of Sciences of the United States of America **109**, 8161-8166.

Figure 1

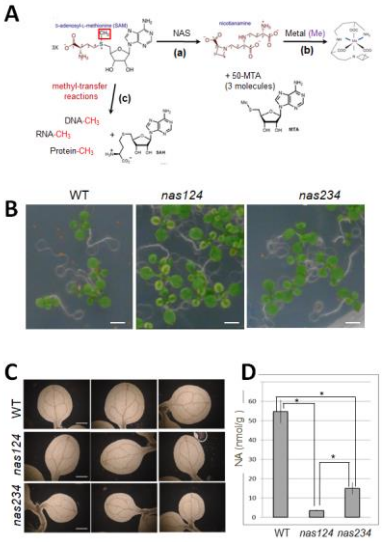
A
NAS
(a)
Metal (Me)
(b)
methyl-transfer reactions
(c)
DNA-CH3
RNA-CH3
Protein-CH3
+ 5'-MTA
(3 molecules)
B
WT
nas124
nas234
C
WT
nas124
nas234
D
NA (nmol/g )
WT
nas124
nas234

Figure 2

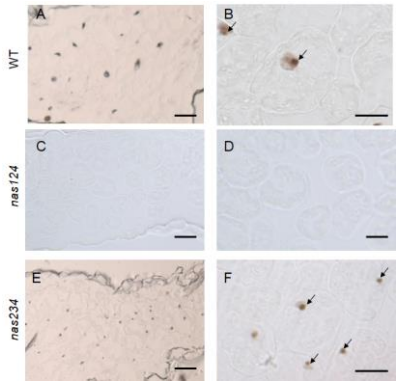

Figure 3

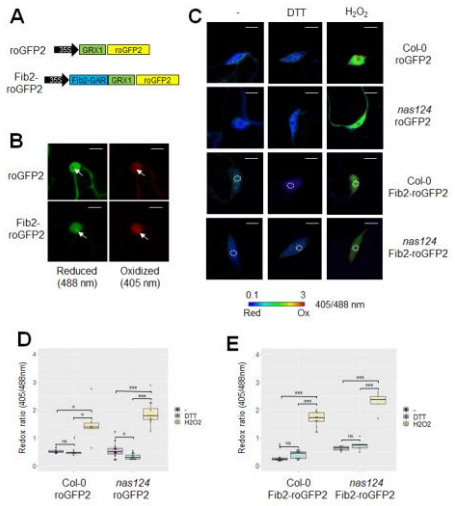
A
roGFP2
GRX1
roGFP2
Fib2-roGFP2
Fib2-CAR
GRX1
roGFP2
B
roGFP2
Fib2-roGFP2
Reduced (488 nm)
Oxidized (405 nm)
C
-
DTT
H2O2
Col-0 roGFP2
nas124 roGFP2
Col-0 Fib2-roGFP2
nas124 Fib2-roGFP2
0.1
3
Red
Ox
405/488 nm
D
Redox ratio (405/488nm)
DTT
H2O2
Col-0 roGFP2
nas124 roGFP2
E
Redox ratio (405/488nm)
DTT
H2O2
Col-0 Fib2-roGFP2
nas124 Fib2-roGFP2

Figure 4

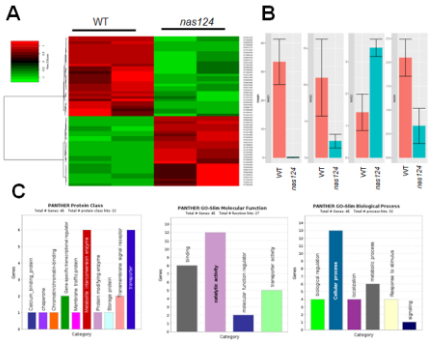

Figure 5

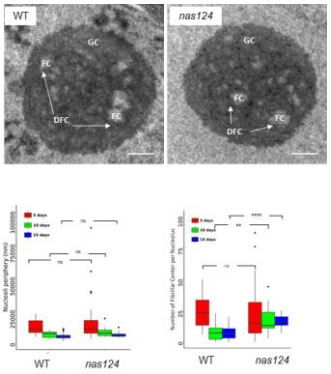

Figure 6

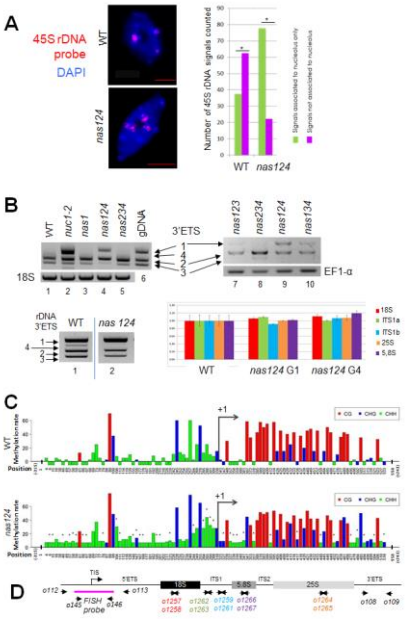
A
45S rDNA probe
DAPI
WT
nas124
Number of 45S rDNA signals counted
WT
nas124
B
WT
nuc1-2
nas1
nas124
nas234
gDNA
18S
3'ETS
nas123
nas234
nas124
nas134
EF1-α
rDNA 3'ETS
WT
nas 124
WT
nas124 G1
nas124 G4
18S
ITS1a
ITS1b
25S
5.8S
C
WT Methylation rate
nas124 Methylation rate
Position
+1
CG
CHG
CHH
D
TIS
5'ETS
18S
ITS1
5.8S
ITS2
25S
3'ETS
o112
o113
o145
FISH probe
o146
o1257
o1258
o1262
o1263
o1259
o1260
o1261
o1266
o1267
o1264
o1265
o108
o109

Figure 7

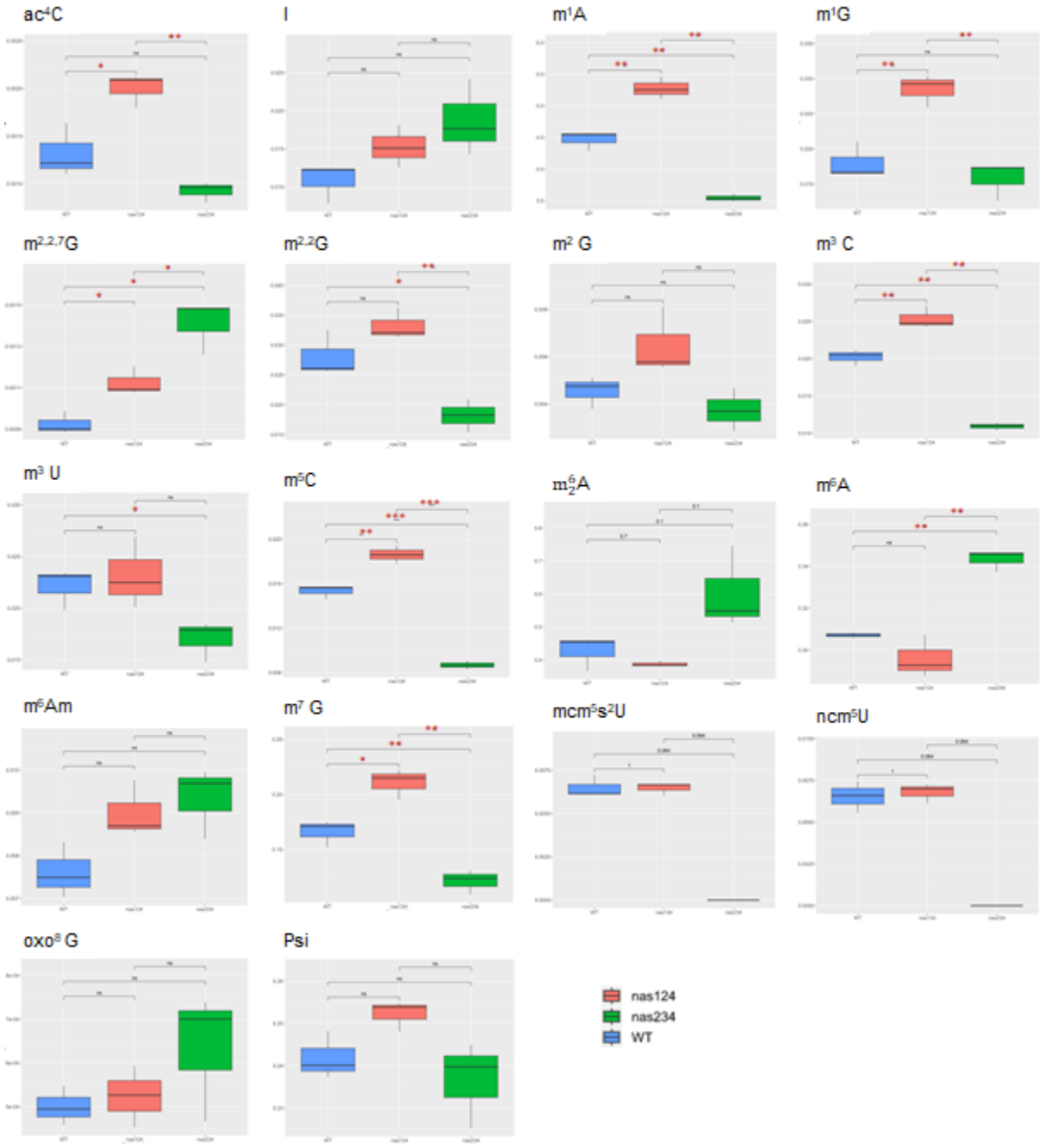
ac4C
I
m1A
m1G
m2,2,7G
m2,2G
m2 G
m3 C
m3 U
m5C
m62A
m6A
m6Am
m7 G
mcm5s2U
ncm5U
oxo8 G
Psi
nas124
nas234
WT